Microstructure behavior of Al–Mg–Sc alloy processed by ECAP at elevated temperature

O. Sitdikov [a,b,*], T. Sakai [c], E. Avtokratova [b], R. Kaibyshev [d], K. Tsuzaki [e], Y. Watanabe [a]

[a] *Nagoya Institute of Technology, Department of Engineering Physics, Electronics and Mechanics, Nagoya 466-8555, Japan*
[b] *Institute for Metals Superplasticity Problems, Khalturina 39, Ufa 450001, Russia*
[c] *UEC Tokyo, University of Electro-Communications, Chofu, Tokyo 182-8585, Japan*
[d] *Belgorod State University, Belgorod 308034, Russia*
[e] *National Institute for Materials Science, Tsukuba 305-0047, Japan*

Abstract

Microstructural evolution taking place during equal channel angular pressing (ECAP) was studied in a coarse-grained Al–6% Mg–0.4% Mn–0.3% Sc alloy at 300 °C ($\sim 0.6T_m$). Samples were pressed to strain 12 and quenched in water after each pass. ECAP at moderate-to-high strains leads to formation of a bimodal grain structure, with grain sizes of about 1 and 8 μm and volume fractions of 0.3 and 0.6, respectively. The development of new-grained regions has been shown to result from the concurrent operation of the continuous dynamic recrystallization that occurs during deformation and the static recrystallization that occurs by the exposure of the as-deformed material in the die kept at 300 °C and/or reheating between pressings. The microstructural development is discussed in terms of the enhanced driving force for recrystallization, resulting from the evolution of high-density dislocation substructures due to localization of plastic flow and inhibition of recovery in the present alloy.

Keywords: Aluminum; Severe plastic deformation; High temperature; Grain refining; Annealing

1. Introduction

In the past decade, many materials scientists and metallurgical engineers have shown considerable interest in the fabrication of ultrafine-grained Al alloys due to the fact that the ultrafine-grained microstructures offer some advantages for the improvement of mechanical and physical properties that may be successfully utilized in industrial applications [1]. Equal channel angular pressing (ECAP) is one of the methods emerging now for producing such microstructures that incorporates the concept of intense plastic straining (IPS), i.e. when ultrahigh strains can be imposed on the worked material without a change in its shape or dimensions [1–5].

There have been several works to date [1–24] showing that ECAP at low-to-high temperatures can be very effective for grain refinement in numerous Al alloys. During cold-to-warm ECAP, some low-to-medium angle subboundaries, sometimes called deformation/microshear bands or geometrically necessary boundaries [25], may be generated in the original grain interiors at relatively low strains due to high strain heterogeneity and result in grain subdivision [4,5,7,18,19,23]. They are progressively transformed into high-angle boundaries (HABs) with further deformation, leading to the full development of new submicrocrystalline grain structures at large strains. It is widely acknowledged that these new grains are evolved in accordance with strain-induced continuous reactions, which are similar to continuous dynamic recrystallization (cDRX) [26,27]. At the same time, only a limited number

of studies have dealt with the evolution process during ECAP at elevated temperatures. As a result, the mechanisms of grain refinement during warm-to-hot ECAP are currently a matter of debate and are not clear. It is considered that the microstructural development in Al alloys under increasing-temperature ECAP conditions can be mainly affected by an increased rate of dynamic recovery, which enhances the rearrangement of the dislocation substructures and assists the formation of new, coarser and more equiaxed (sub)grains [9,13,16,17]. Unfortunately, the major factors controlling such microstructural development are still unknown due to the lack of related experimental data, especially for heavily alloyed Al alloys.

It is known that Al–Mg–Sc alloys belong to a class of advanced structural materials that have been developed in recent years with the purpose of improving some of the service properties of non-heat-treatable Al–Mg alloys [28]. Scandium is a unique alloy addition to aluminum in that it may form an equilibrium, thermally stable, coherent Ll_2 phase (Al_3Sc) with Al. This phase can be extremely effective in dislocation pinning and thus provides a high strengthening effect [29]. At the same time, this alloy is hard to deform by cold working because of its high yield stress and relatively low ductility at ambient temperature [11,15,28]. In contrast, by increasing the pressing temperature, the plastic workability of Al–Mg–Sc alloys may be improved and additional benefits may be obtained from the decrease in the strength of the material. With these advantages, IPS performed under warm-to-hot deformation conditions could be a very promising technical procedure with great commercial potential (e.g. [30,31]). Accordingly, an evaluation of the potentiality of grain scaling in Al–Mg–Sc alloys during ECAP at elevated temperatures seems to be very important for commercial applications.

The aim of the present research, therefore, was to study the microstructural evolution of a commercial Al–6% Mg–0.3% Sc alloy subjected to ECAP at 300 °C ($\sim 0.6T_m$). In the current work, the starting material was a pre-extruded rod with an initially partially recrystallized microstructure resulting from previous extrusion and annealing operations, which may be the most suitable object for investigations into microstructural changes during ECAP under industrial conditions [32]. Specific attention was given to clarify the main factors promoting grain refinement in this alloy at an elevated temperature and to discuss the effect of deformation temperature on the mechanisms of new grain formation in detail.

2. Experimental

The alloy used had the following chemical composition (in mass%): 6Mg, 0.4Mn, 0.3Sc, 0.2Si, 0.1Fe and the balance Al. It was fabricated by casting in a steel mold at the Kamensk-Uralsk Metallurgical Works (Russia) and then homogenized at 520 °C for 48 h. Extrusion was performed at 390 °C to a strain of about 0.7, followed by annealing at 400 °C for 1 h. After extrusion and annealing, the alloy was composed of partially recrystallized equiaxed grains, with an average size of 4.4 μm and a volume fraction of about 0.35 developed along the boundaries of coarse elongated grains lying parallel to the extrusion axis (see Fig. 2a). The size of these coarse grains was varied from 150 to 200 μm and from 50 to 100 μm in the longitudinal and transverse direction, respectively. Nanoscale dispersion particles in the present material were identified as coherent Al_3Sc dispersoids, having a size of 10–20 nm [32].

Samples for ECAP were machined parallel to the extrusion axis into rods with a diameter of 20 mm and a length of about 100 mm. ECAP was carried out at 300 °C using a die circular in cross-section with a diameter of 20 mm. The die had an L-shaped channel with an angle of 90° between the two channels and an angle of 0° at the outer arc curvature at the point of intersection. These angles led to a strain of about 1 in each passage through the die. A heating jacket was put on the die and the pressing temperature was controlled to be within ±5 °C of 300 °C. Samples were pressed repeatedly to a strain of 12 using route A, i.e. the orientation of billet was not changed at each pass. Route A was selected in the present work because it is the most efficient processing route for forming a fine grain structure with a large fraction of HABs (e.g. [12]). Moreover, this is the simplest method of ECAP and, hence, could be the most suitable for grain refinement under industrial conditions. The ECAP was performed in a hydraulic press operating at a pressing speed of $\sim 6\ mm\ s^{-1}$. The samples pressed were quenched in water after each deformation pass and then reheated at 300 °C for 45 min before the next ECAP, as shown in Fig. 1. The mean time interval between the starting ECAP in each pass and immersion of the sample after pressing into water was about 1.5 min.[1]

Samples for optical microscopy, electron backscattering diffraction pattern (EBSP) and transmission electron microscope (TEM) analyses were cut from central parts of the pressed rods in the longitudinal section parallel to the pressing direction. Samples for optical microscopy were annealed at 170 °C for 4 h in order to decorate HABs by secondary Al–Mg phase particles [20,32]. These grain-boundary precipitates were then revealed by etching with a standard Keller's reagent. The metallographic observations were carried out using a Nikon L-150 optical microscope and a JSM840 scanning electron microscope (SEM). (Sub)grain boundary misorientation distributions were obtained from EBSP using an LEO1530 SEM and a JSM6500 SEM. Over the misorientation parameters measured by EBSP, boundaries with misorientation less than 2° were not taken into account. Also "recrystallized" and "deformed" fractions were evaluated by EBSP measurements using Channel 5 EBSP software [33]. These components in orientation imaging microscopy (OIM) maps were

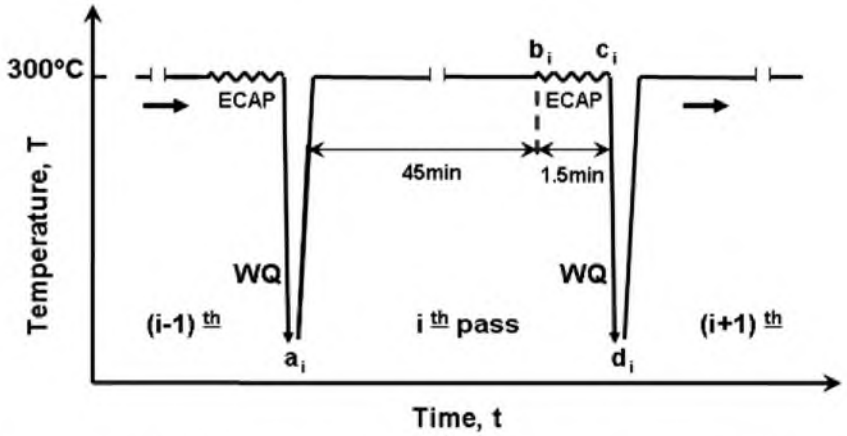

Fig. 1. Schematic representation for the cyclic ECAP procedure. a_i–b_i: (re)heating and exposure of samples at 300 °C before ECAP during 45 min; b_i–c_i: ECAP at 300 °C; c_i–d_i: quenching of as-ECAPed samples in water (WQ). The d_is indicate points after ECAP at which the structure observations were carried out.

determinated automatically in accordance with the following steps.

(i) First, the subgrains and grains were determined to be the areas surrounded by boundaries with misorientations of $2° \leqslant \theta < 15°$ and $\theta \geqslant 15°$, respectively.
(ii) Then the internal average misorientation angle was measured within each grain.
(iii) If the internal misorientation in a grain exceeded 2°, the grain was classified as being "deformed".
(iv) If the grains consisted of subgrains, whose internal misorientation was less than 2° but whose misorientation from subgrain to subgrain was above 2°, the grains were classed as "substructured".
(v) All the remaining grains were classified as "recrystallized".

Specimens for TEM examination were mechanically ground to a thickness of about 200 μm and electropolished at 20 V in a solution of 30% HNO_3 and 70% CH_3OH at a temperature of −30 °C using a Tenupol-3 twin-jet polishing unit. They were then examined using a JEOL-2000EX TEM.

3. Results

3.1. Deformation microstructures

A series of typical microstructures is represented in Fig. 2: (a) before ECAP ($\varepsilon = 0$) and (b)–(d) evolved during ECAP to $\varepsilon = 1$–12. It is seen that the original coarse grains presented in the initial structure (Fig. 2a) are pancaked along the pressing direction (PD) and, concurrently, new, finer grains are created by ECAP, first in the former mantle regions and then over the whole original coarse grains (Fig. 2b–d). It is important to note that, at all strains investigated, the newly evolved ECAP microstructure is highly non-uniform and consists of two structural components with a bimodal distribution of grain size. One of them comprises fine-grained bands, which appear in dark-color regions aligned along PD, as arrowed in Fig. 2b–d. The size of the crystallites evolved in these bands was about 1 μm, as shown at larger magnification in Fig. 2d. The other is composed of relatively coarse grains of about 8 μm that maintain an essentially equiaxed shape after each ECAP pass. In addition to these, deformed grains were also present in the microstructure. At moderate-to-high strains above 8, the volume fractions of fine- and coarse-grained components were as high as 0.3 and 0.6, respectively.

The typical data derived from EBSP analysis are summarized in Figs. 3–5. Fig. 3 represents the structures observed by OIM at (a) $\varepsilon = 0$, (b) $\varepsilon = 1$, (c) $\varepsilon = 2$, (d) $\varepsilon = 4$ and (e) $\varepsilon = 12$. Here the different grayscale levels indicate the different crystallographic orientations, and the differences between neighboring grid points $2° \leqslant \Theta < 5°$, $5° \leqslant \Theta < 15°$ and $\Theta \geqslant 15°$ are marked by narrow white, narrow gray and bold black lines, respectively. It is seen in Fig. 3a that the alloy just before ECAP, i.e. at $\varepsilon = 0$, contains networks of dislocation sub-boundaries with $2° \leqslant \Theta < 15°$ in the coarse original grain interiors. Their average misorientation angle, Θ_{ave}, was about 6.5° (see Figs. 9 and 10). The size of the crystallites fragmented by those sub-boundaries was in the range from 3 to 30 μm. In addition, mixed arrays of (sub)grain boundaries with an average misorientation angle of about 26.4° were present in original mantle regions. The fractions of HABs, f_{HABs}, were 0.05 and 0.62 in the grain interiors and mantle regions, respectively.[2] During ECAP, highly inhomogeneous deformation is introduced into the present alloy, as shown in Fig. 3b–e, leading to high strain and misorientation gradients and also to new grains and deformation substructures that consist of sub-boundaries

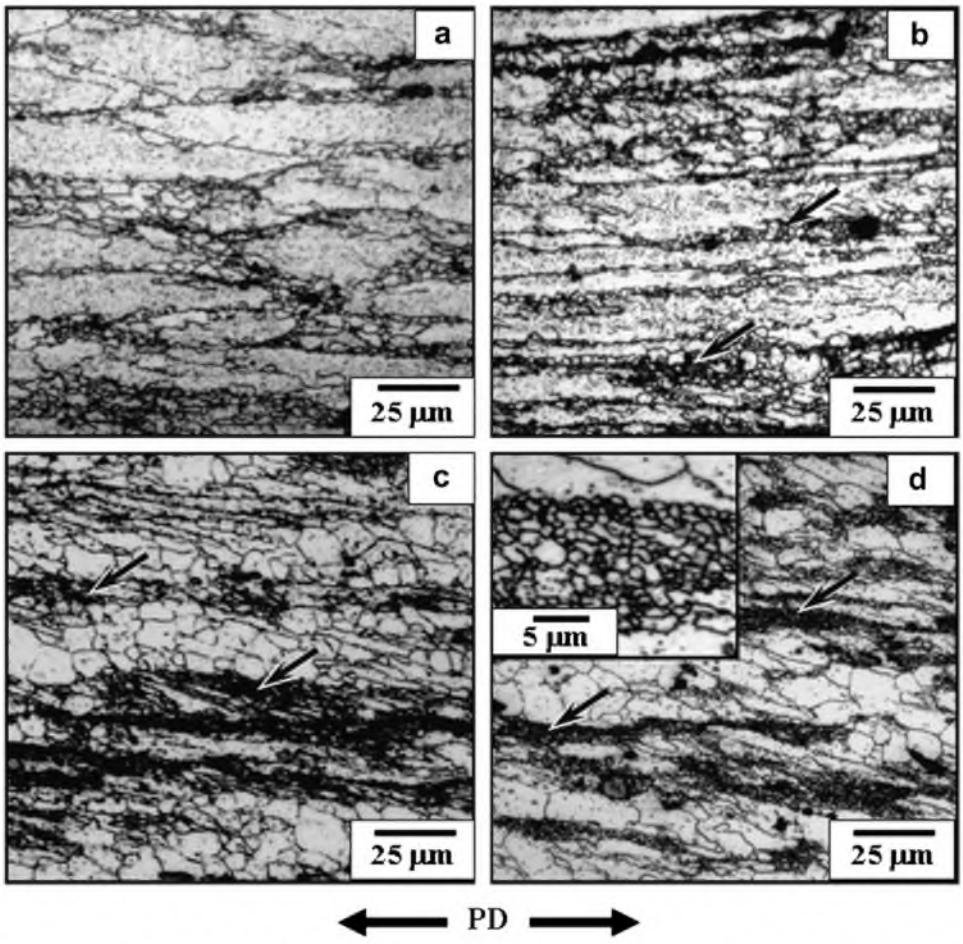

Fig. 2. Typical optical microstructures developed in Al–6% Mg–0.3% Sc–0.4% Mn alloy after ECAP: (a) $\varepsilon = 0$; (b) $\varepsilon = 1$; (c) $\varepsilon = 4$; and (d) $\varepsilon = 12$. Dark regions arrowed in (b)–(d) are composed of fine equiaxed crystallites with a mean size of around 1 μm, as shown at larger magnification in the portion outlined in the upper left corner of (d).

with low-to-medium and even high angle misorientations, finally followed by a formation of the bimodal grain structure at high strains (see Fig. 3e). The main important features of such microstructural development can be described as follows.

(i) First, Fig. 3b shows that, after the first ECAP pass, the dislocation sub-boundaries that are formed in the original grain interiors develop very non-uniformly on the mesoscopic level. Most of them are not sharply defined in the grain centers, where significant orientation gradients exist, suggesting that they may be rather diffuse dislocation walls. At the same time, several sets of intense sub-boundaries can be observed more clearly in the areas adjoining predominantly the original mantle regions, where frequently elongated new fine grains are evolved. At larger strains ($\varepsilon = 2$–4), the deformation microstructures in the grain interiors comprise more regular arrays of dislocation sub-boundaries that are developed in various directions (Fig. 3c and d). They fragment the original grain into small, separate misoriented domains, some of which are transformed into new fine grains, frequently in the grain boundary regions and occasionally in the grain interiors (see Fig. 3d). At the highest strain level investigated, i.e. $\varepsilon = 12$ (Fig. 3e), such new fine grains mostly surrounded by HABs are frequently but inhomogeneously developed in colonies accompanied with evolution of relative coarse crystallites with moderate-to-high angle boundary misorientations. The latter contain areas with high misorientation gradients and probably correspond to remnant parts of original grains, which survive to high plastic strains without subdivision [23].

(ii) Fig. 4 represents the distribution of typical point-to-point ($\Delta\Theta$) and cumulative (point-to-origin) ($\Sigma\Delta\theta$) misorientations developed in the present alloy at moderate-to-high strains along the lines (a) T_1; (b) T_2; and (c) T_3, indicated in Fig. 3c, d and e, respectively. The values of $\Delta\Theta$ and $\Sigma\Delta\Theta$ define the misorientations evolved by 0.1 μm steps relative to the previous point and to the first point, respectively. It can be seen that $\Delta\Theta$ in Fig. 4a does not generally exceed 2° except for some spots with $\Delta\Theta \geqslant 4$–5°,

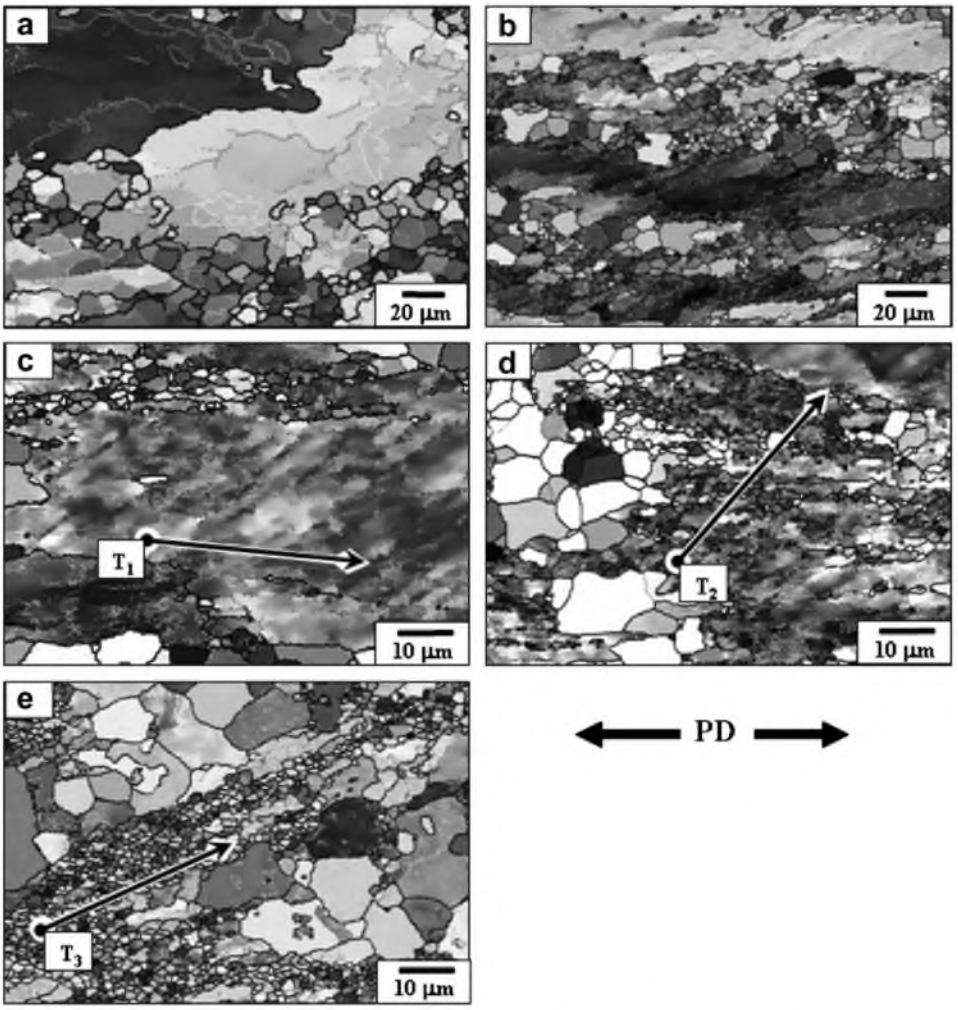

Fig. 3. Typical OIM microstructures developed in Al–6% Mg–0.3% Sc–0.4% Mn alloy during ECAP at $T = 300$ °C: (a) $\varepsilon = 0$; (b) $\varepsilon = 1$; (c) $\varepsilon = 2$; (d) $\varepsilon = 4$; and (e) $\varepsilon = 12$.

which correspond to the deformation-induced dislocation sub-boundaries mentioned in Fig. 3. It is also remarkable to see that $\Sigma\Delta\Theta$ changes discontinuously and crystal orientations alternate at the same places. This indicates that heterogeneous deformation that occurs in the present alloy during ECAP leads frequently to local lattice rotations followed by formation of dislocation sub-boundaries. These may correspond to the boundaries of deformation or microshear bands, which are able to be introduced into Al alloy even under elevated temperature deformation conditions, as discussed in detail elsewhere [12,32,34]. Some of these boundaries approach the large angle misorientations beyond 10–15° and transform into HABs (Figs. 3d and 4b). Fig. 4c also shows the variation of the misorientations in fine-grained regions developed at $\varepsilon = 12$. It can be seen that the density and the misorientation angle of the strain-induced sub-boundaries increase during ECAP, and new HABs with misorientations ranging from 15° to beyond 50° are developed in certain areas of deformed microstructure.

(iii) Fig. 5 displays a typical distribution of "recrystallized", "deformed" and "substructured" fractions in the present alloy at (a) $\varepsilon = 1$ and (b) $\varepsilon = 8$. These fractions were determined depending on the value of the internal misorientation angle measured within each grain (see Section 2). In the maps in Fig. 5, the "fully recrystallized" grains are shown in white, "deformed" regions show up as dark and "substructured" grains are gray.[3] Fig. 5a shows that areas with a size of about 1 μm and an internal misorientation of more than 2° are frequently developed in the mantle regions after the first ECAP pass. This indicates that

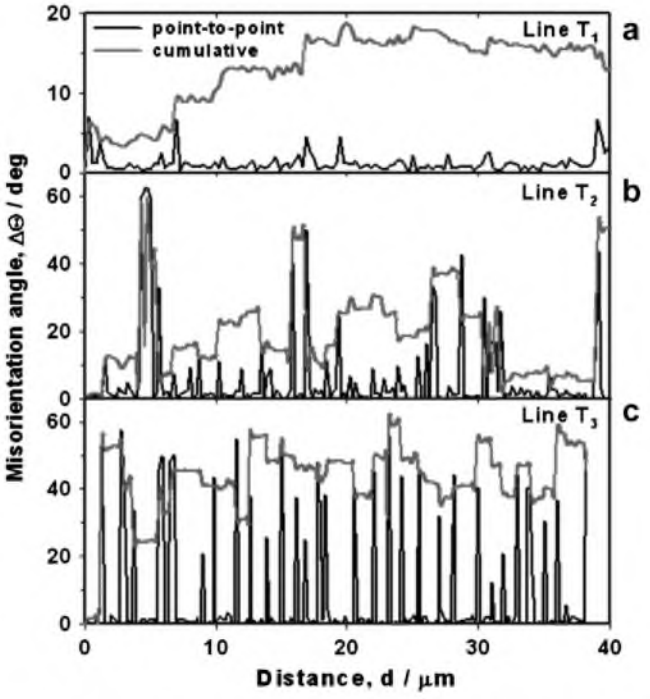

Fig. 4. Typical point-to-point and cumulative misorientations developed in Al–6% Mg–0.3% Sc–0.4% Mn alloy during ECAP at $T = 300$ °C along the lines (a) T_1, (b) T_2 and (c) T_3 indicated in Fig. 3. Note the different scale in (a).

the internal lattice distortion angle in these areas may be more than 2° μm^{-1}, which corresponds to the minimal stored dislocation density of about 1–4×10^{14} m^{-2} [10,25]. Such highly distorted areas may also develop frequently in some local regions within the strain-hardened original grains after large strains (Fig. 5b). This suggests that dynamic/static recovery hardly occurs in the present alloy at 300 °C and that sequential structural changes that occur during repeated ECAP are mainly affected by the strong strain accumulation that is applied in each ECAP pass.

(iv) Finally, it can be seen in Figs. 3 and 5 that the rather coarse recrystallized grains mentioned in Fig. 2 appear frequently after the first ECAP pass in the fine-grained structure present in the original mantle regions (see Figs. 2a and 3a). The fraction of these grains increases rapidly with repeated ECAP to replace parts of the deformed microstructure in the grain interiors that especially exhibit a high level of lattice distortion and/or high misorientation gradients. Note that such grains are classified by OIM software as "recrystallized" grains because their average internal lattice distortion angle does not exceed 0.25° μm^{-1} (i.e. their internal misorientation angle is <2° within a grain size of about 8 μm). In addition,

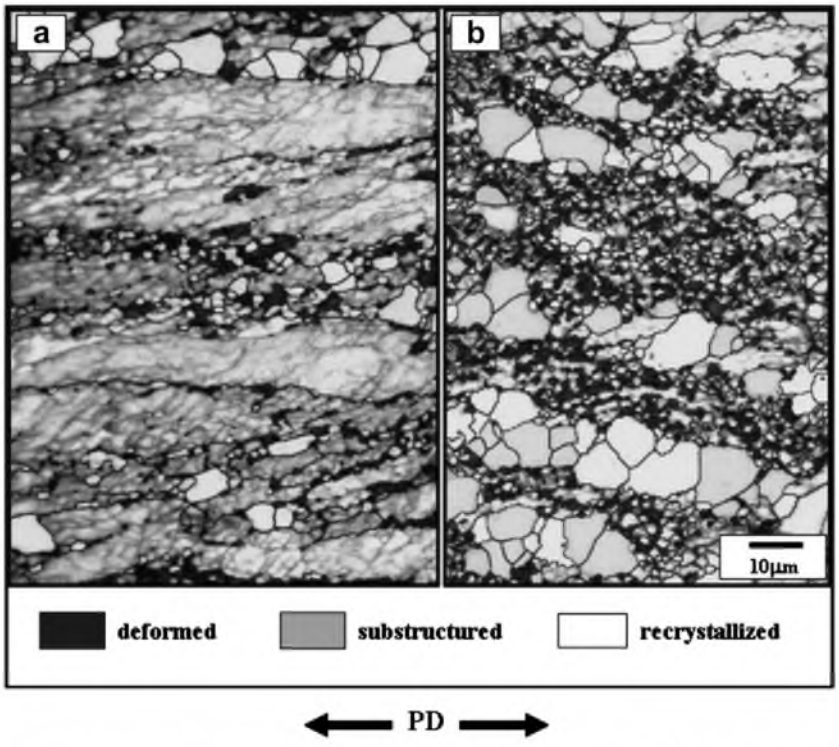

Fig. 5. Distribution of deformed, substructured and recrystallized fractions in Al–6% Mg–0.3% Sc–0.4% Mn alloy after ECAP to (a) $\varepsilon = 1$ and (b) $\varepsilon = 8$. In these maps, a grain is classified as being "deformed" if its internal average misorientation angle exceeds 2°. A grain is classified as "substructured" if it consists of subgrains whose internal misorientations are under 2°, but whose boundary misorientations exceed 2°. All the remaining grains are classified as "recrystallized".

their pattern quality is relatively high; i.e. their coincidental index (CI) and image quality (IQ) can be measured to be always more than 0.5–0.6 and 100, respectively. This may also be good evidence of their low defect density [33]. Note that some of the grains show interior low-angled boundaries, as seen in Fig. 3. However, by referring to the almost identical equiaxed shape of most of the grains, which appears in all stages of deformation (see Fig. 2), we can assert that they are reproduced during each ECAP pass by static, rather than dynamic, processes.

3.2. Texture changes

Fig. 6 shows the typical inverse pole figures of the PD obtained from the EBSP data, which were plotted for (a) $\varepsilon = 1$, (b) $\varepsilon = 2$ and (c) $\varepsilon = 12$. The "deformed/fine-grained" and "recrystallized" microstructures were cropped on OIM maps in original grain interiors and in mantle regions, respectively, and then analyzed separately. It is seen in Fig. 6a that, after the first ECAP pass, a strong fiber texture is evolved in the grain interiors, in which the maximums of the orientation density occur roughly between ⟨315⟩, ⟨213⟩ and ⟨313⟩ and also between ⟨212⟩, ⟨535⟩ and ⟨335⟩, and, additionally, the broad bands of the orientations fill almost whole ~15° ranges between these directions.[4] During the second pass through the die (Fig. 6b), the deformation microstructure is reoriented between ⟨013⟩ and ⟨535⟩, and, with further straining, tends to rotate toward the line from ⟨001⟩ to ⟨111⟩ (see Fig. 6c); this may be comparable to the structural changes that occur during cold rolling [35]. However, it is remarkable to see that the rather strong crystallographic texture that is observed in the grain interiors at $\varepsilon = 1$ is changed to a roughly random one by transition to the mantle regions (Fig. 6a). It is also gradually destroyed with increasing strain (Fig. 6b and c). As the result, some diffused and nearly random microstructures are finally formed at the highest ECAP strains in both structural components (Fig. 6c). Note that such structural behavior may contradict the strong texture strengthening, which was reported, for instance, for cold- and cold-to-warm ECAP of Al alloys, Ag and Cu at large strains [8,14,36,37]. On the other hand, a weakening and/or randomization of texture was often observed during conventional or severe hot straining of some Al alloys (e.g. [34,38]). These may have resulted from (sub)grain rotation, which frequently takes place during warm-to-hot deformation, as will be discussed in Section 4.

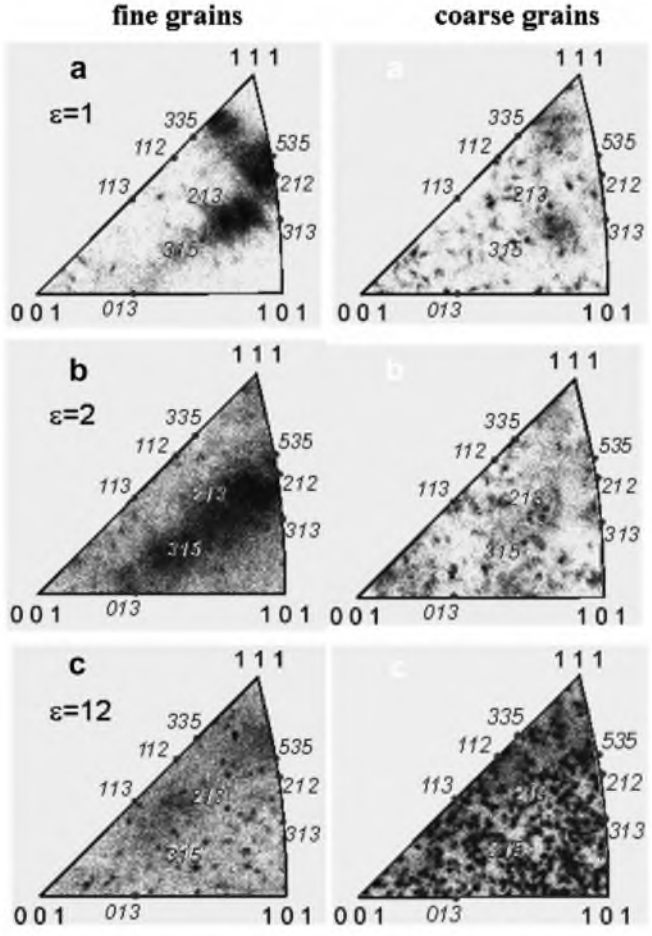

Fig. 6. Typical inverse pole figures showing the textures evolved in the fine- and coarse-grained regions in Al–6% Mg–0.3% Sc–0.4% Mn alloy at various ECAP strains at 300 °C: (a) $\varepsilon = 1$; (b) $\varepsilon = 2$; and (c) $\varepsilon = 12$.

3.3. TEM microstructures

Typical TEM microstructures evolved in the samples pressed to $\varepsilon = 4$ (see Fig. 2c) are illustrated in Fig. 7. These show (a) and (b) banded dislocation arrays with areas of high density of dislocations; (c) well-developed (sub)grain structures composed of crystallites separated by moderate-to-high angle dislocation (sub)boundaries (see the SAED pattern inserted); and (d) coarse recrystallized grains, which are formed in various parts of the ECAPed material at moderate-to-high strains. Note that:

(i) the dislocation density in some banded areas with large amounts of lattice dislocations introduced by ECAP was evaluated as $1–3 \times 10^{14}\ m^{-2}$, although it may often be so high that separate lattice dislocations can hardly be resolved by the TEM technique, as shown in Fig. 7a and b. This may be consistent with the high lattice distortion data evaluated by OIM analysis (see Section 3.2)[5];

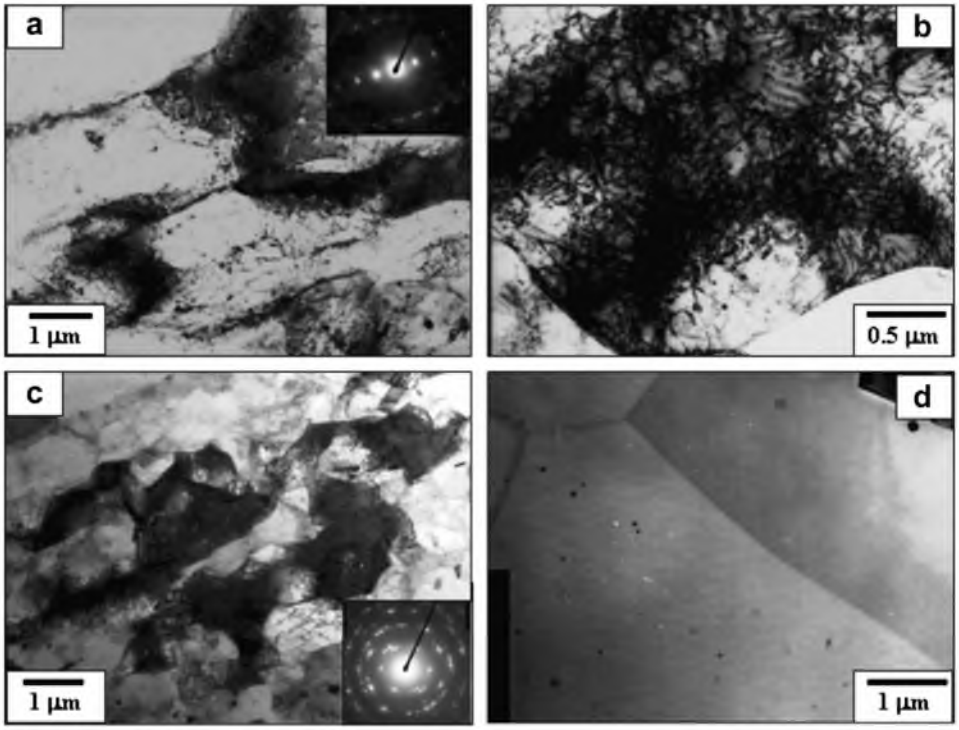

Fig. 7. Typical TEM microstructures and the diffraction patterns of Al–6% Mg–0.3% Sc–0.4% Mn alloy evolved during ECAP at $T = 300$ °C and $\varepsilon = 4$.

(ii) there are relatively high dislocation density values within small (sub)grains represented in Fig. 7c, which contrast with the virtually dislocation free interiors of coarse recrystallized grains denoted in Fig. 7d.

Thus, Fig. 7a and b shows the development of dislocation sub-boundaries with high dislocation density and indicates the inability of the material to recover completely within these substructures; Fig. 7c and d provides, in turn, some independent evidence that new grains may form both dynamically and statically by mechanisms of evolution of dislocation sub-boundaries and nucleation and limited grain growth, respectively.

Fig. 8 represents the typical features of the distribution of the secondary phase dispersion particles in (a) deformed and (b) statically recrystallized areas at a strain of 4. It is seen in Fig. 8a that the spatial distribution of the dispersion particles in the deformed structure is rather homogeneous and most of them demonstrate a well-known "coffee-bean"-like contrast, which can be attributed to the coherent dispersoids [39]. Hence, they can be clearly recognized as the coherent $L1_2$–Al_3Sc particles (see Section 2). It is important to note that the size of these particles is unaltered during ECAP and is about 10–20 nm. Also, there is a relatively high density of tangled lattice dislocations in such deformed microstructure which interact with the dispersoids. This suggests that the dispersoids can trap the dislocations, significantly inhibiting recovery even at elevated temperatures. On the other hand, such fine precipitates can be rarely observed in the regions of the statically recrystallized structure (Fig. 8b). The particles, which are only present here, have an unexpectedly large size of about 60–70 nm and exhibit scarcely any evidence for coherency with the surrounding Al matrix. They are located both in the grain interiors and at the boundary regions of coarse recrystallized grains (see Figs. 7d and 8b), and some of them interact strongly with the grain boundaries, providing effective grain boundary pinning.

3.4. Microstructure parameters

Fig. 9 a–d and a′–d′ represents changes in the misorientation distributions of the (sub)grain boundaries in the deformed/fine-grained and coarse-grained structures developed in the original grain interiors and in the mantle regions, respectively, at (a and a′) $\varepsilon = 0$; (b and b′) $\varepsilon = 1$; (c and c′) $\varepsilon = 4$; and (d and d′) $\varepsilon = 12$. It is seen in Fig. 9a–c that most of the boundaries that developed in the grain interiors before and after the first four passes of ECAP (i.e. at $\varepsilon = 0$–4) exhibit low-to-medium angle misorientations from 5° to 15°. With further deformation, the fraction of low- and moderate-angle boundaries gradually decreases and that of high-angle ones, f_{HABs}, conversely increases to about 0.6 in fine-grained regions (Fig. 9d); this is directly connected with the evolution of new fine grains. In comparison, the relative number of high- and low-angled boundaries in mantle regions varies with strain in a complex manner, as shown in Fig. 9a′–d′. First, the fraction of HABs in these regions drops due to the increase in the number of low-angled boundaries during the first pass through the die and then rises rapidly with further ECAP and saturates at moderate strains, thus the histograms plot-

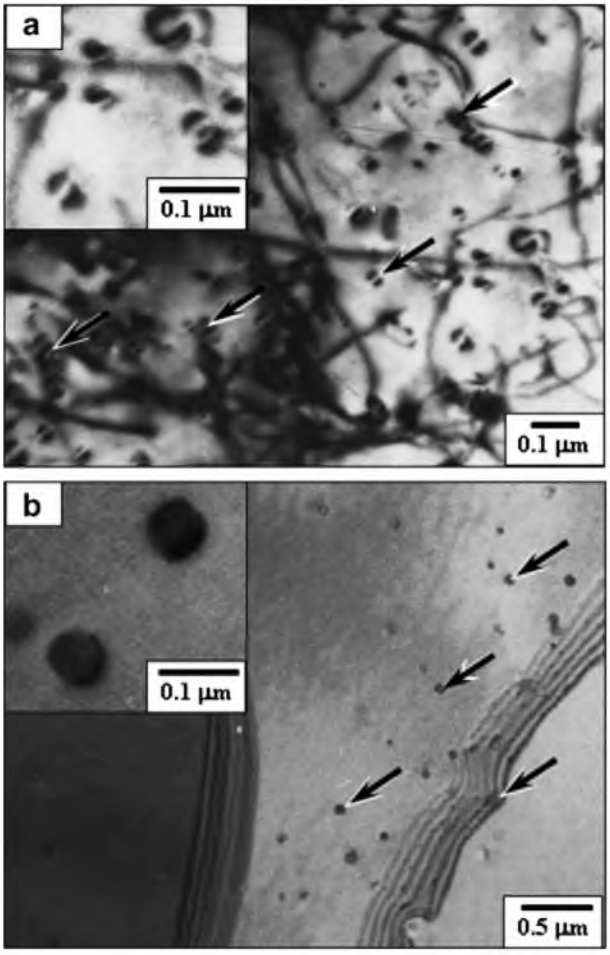

Fig. 8. Typical TEM images showing the distribution of nanoscale dispersion particles in Al–6% Mg–0.3% Sc–0.4% Mn ECAPed at 300 °C and $\varepsilon = 4$: (a) non-recrystallized and (b) recrystallized regions.

ted at strains beyond 4 show the relative abundance of HABs and scarcely change with further increasing strain (Fig. 9c′ and d′). It is interesting to note that at the highest ECAP strain, i.e. $\varepsilon = 12$, the angular characteristics of the boundaries developed in the grain interiors and in the mantle regions are roughly similar (see Fig. 9d and d′) and that their average misorientation, Θ_{ave}, which is about 24–25°, remains significantly less than that of 40.7°, predicted by Mackenzie for randomly misoriented polycrystalline aggregates of cubic metals [40]. The latter suggests that while the large-scale microstructures are mainly composed of HABs, the deformed structures with a fraction of low- and medium-angle boundaries persist in the both regions.

Strain dependencies of the average misorientations, Θ_{ave}, are summarized in Fig. 10. It can be seen that the Θ_{ave} of the (sub)grain boundaries that are developed in the mantle regions first drops from 26.4° at $\varepsilon = 0$ to 15.2° at $\varepsilon = 1$ and then rapidly increases with increasing strain from 1 to 4 followed by saturation at 26.5° ± 1.5° at large strains above 4. At the same time, the Θ_{ave}, which was measured in the original grain interiors, increases from 6.5° at $\varepsilon = 0$ to above 20° at $\varepsilon \sim 8$ and finally approaches a saturation value of 24 ± 1°.

Fig. 11 represents the strain dependencies of (a) the volume fractions, V_{rex}, and (b) the average grain sizes, d_{rex}, of the new "fine" and "coarse" grains developed during ECAP (full symbols). Also, the data for the microstructure obtained after subsequent static annealing for 45 min at 300 °C, which corresponds to the reheating between ECAP passes, i.e. points $b_{(i+1)}$s in Fig. 1, are represented by open symbols for comparison in Fig. 11. It is seen in Fig. 11 that in the as-ECAPed state, the V_{rex} of the "fine" grains increases continually from a value of 0.12 at $\varepsilon = 1$ to 0.33 at $\varepsilon = 12$, while the size of these grains monotonically decreases from about 1.3 μm to about 1 μm in the strain interval from 1 to 4, followed by saturation at about 0.9–1 μm at $\varepsilon > 4$. The volume fraction of "coarse" grains is increased during ECAP from 0.35, which corresponds to the original grain structure in the mantle regions, to 0.6 at $\varepsilon = 4$, then does not change significantly during further processing to high strains. The size of the "coarse" grains grows during the two first passes through the die from 4.4 μm to become saturated at a value of about 8 μm at $\varepsilon \geqslant 2$, as seen in Fig. 11b.

It can be also seen in Fig. 11 that the "fine-grained" structure that is evolved during ECAP remains almost stable during reheating between passes at all strains investigated, while both the volume fraction and the size of the "coarse" grains are remarkably increased (compare the open and filled symbols in Fig. 11). The latter indicates that these "coarse" grains are repeatedly deformed, renucleated and grow during each ECAP pass, and proceed to grow during reheating between passes. Their volume fraction grows to about 0.75 in the stain interval from 1 to 4 and then stabilizes, so that the sum of the volume fractions of "coarse" and "fine" grains tends to approach to about 0.9–1 at large strains, while their mean size approaches a value of about 12.5 μm during annealing at $\varepsilon = 2$, followed by some additional gradual coarsening to about 15.5 μm at high strains.

4. Discussion

ECAP of the Al–Mg–Sc alloy at 300 °C results in a mixed bimodal grain structure, in which regions composed entirely of fine (sub)grains alternate with regions of coarse recrystallized grains. This suggests that a processing window may exist at this temperature, when the grain refinement during ECAP is accompanied by a simultaneous grain coarsening. It can be noted that such a complex effect of warm-to-hot ECAP on microstructural behavior of Al alloys has not been noticed before, to the best of authors' knowledge, although the sudden formation of a microstructure with an unexpectedly large grain size was previously reported for some heavily alloyed Al alloys ECAPed at $T \sim 300$–400 °C [8,13,21]. On the other hand, similar duplex structures were sometimes formed due to heterogeneous grain coarsening during static annealing of ultrafine-grained Al–Mg alloys produced by cold ECAP (e.g. [4,11,41,42]). The two types of grained structures with

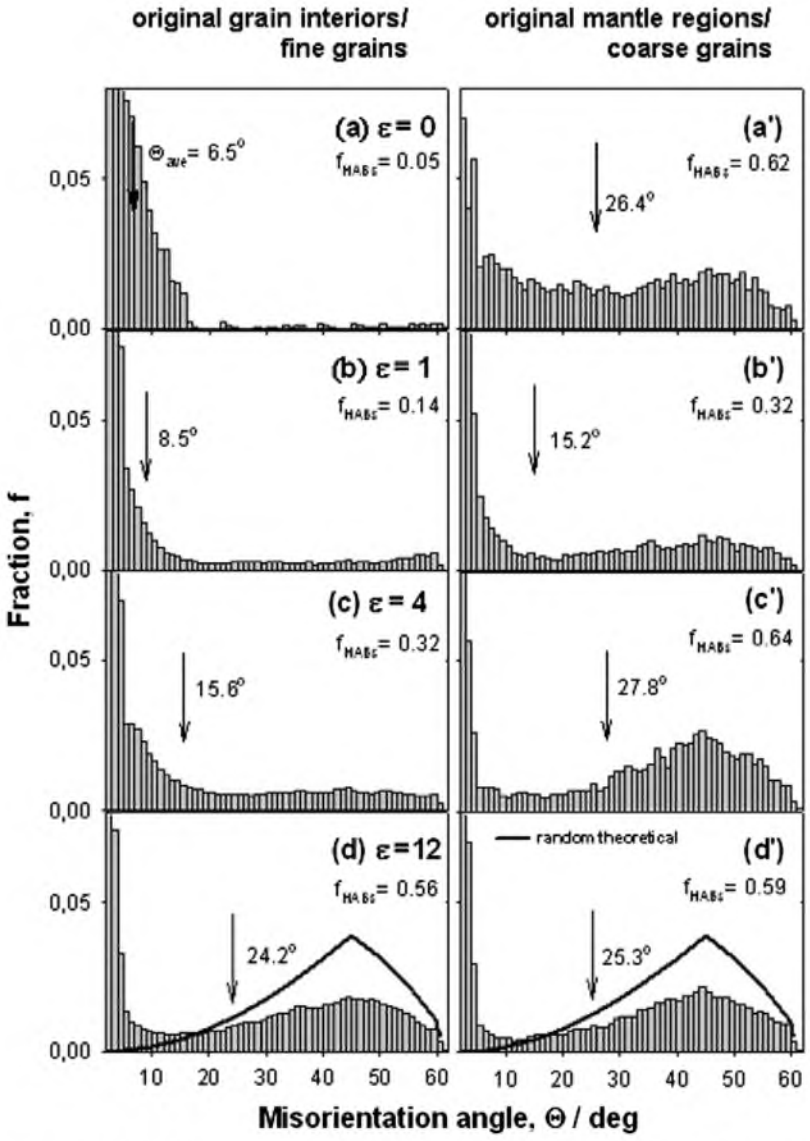

Fig. 9. Changes in misorientation distribution of dislocation and (sub)grain boundaries developed with straining by ECAP in (a–d) fine-grained regions and (a′–d′) coarse-grained regions: (a, a′) $\varepsilon = 0$; (b, b′) $\varepsilon = 1$; (c, c′) $\varepsilon = 4$; (d, d′) $\varepsilon = 12$. Solid lines in (d) and (d′) indicate the random misorientation distribution evaluated by Mackenzie.

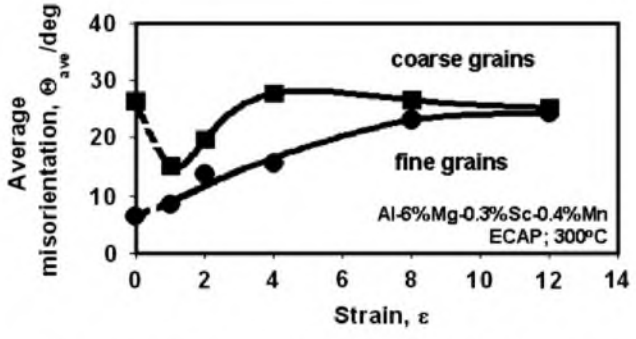

Fig. 10. Strain dependence of the average misorientation, Θ_{ave}, of (sub)grain boundaries developed in the fine- and coarse-grained regions of the Al–6% Mg–0.3% Sc–0.4% Mn alloy during ECAP at 300 °C.

significantly different grain sizes are assumed to originate from different structural mechanisms operated under the present ECAP conditions. In this section, the evolution process of the new fine- and coarse-grained structural components, which are developed in the present alloy during ECAP, will be discussed in detail.

4.1. Evolution of the fine-grained structure during warm-to-hot ECAP

The results described above show that new fine grains with the size of about 1 μm are developed during ECAP of the present alloy due to grain fragmentation process accompanied by frequent evolution of deformation-induced sub-boundaries with low-to-moderate angle misorientation, which can be recognized as the boundaries of deformation bands (DBs) [7,19]. It was recently reported [4,7,10,12,17–19,23,27,32,34,36] that, under IPS conditions at low to high temperatures, original grains can be subdivided by layered dislocation substructures and/or DBs, fol-

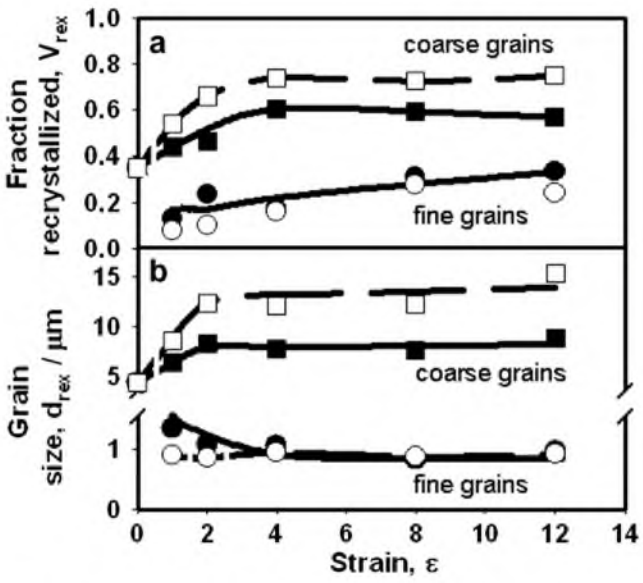

Fig. 11. Strain dependencies of the parameters of the microstructures evolved in fine- and coarse-grained regions after ECAP at 300 °C (full symbols) and subsequent annealing at 300 °C for 45 min (open symbols) (see Fig. 1): (a) the volume fraction of newly evolved grains and (b) the average grain sizes.

lowed by evolution of fine crystallite components at high strain, and such a process may play an important role in grain refinement. During cold-to-warm IPS, the formation of DBs occurs because it is energetically easier for a grain to deform if it is split into DBs, where the number of slip systems required for constrained deformation are fewer than five [4,23]. The DBs may also be formed by grain subdivision as a result of coarse slip associated with shear banding. A mechanism of grain refinement during ECAP can be summarized as follows [12,17,27,34]:

(i) inhomogeneous deformation characteristics of ECAP led to formation of DBs, which are considered to be developed by relaxation of strain gradients resulting from heterogeneous strains introduced by ECAP;
(ii) repeated ECAP results in an increase in the number and misorientation of the boundaries of DBs; their mutual crossing leads to continuous fragmentation of coarse original grains into separate misoriented domains; and
(iii) the boundary misorientations of these domains grow rapidly with increasing strain, followed by their transformation into new grains surrounded by HABs at high strains.

Similar discussion can be applied to describe the microstructural evolution in the current alloy, in which the same structural changes can be clearly revealed (see Fig. 3). A rapid formation of DBs is obviously associated with accommodation of shear strains introduced by ECAP, which result in significant local lattice rotations and/or distortions in the prior grains (see Fig. 5). In the present alloy, the DBs can be frequently developed even at elevated temperature, because there is a strong interaction of the lattice dislocations with Al_3Sc dispersion particles (Fig. 8a) and/or Mg atoms in Al solid solution [6,16,21,43]. This restricts a dislocation rearrangement within the DBs and thus provides a thermal stability of the dislocation substructures introduced by ECAP. Changes in the shearing plane with a respective increase in the number of passes in route A [44] promotes, in turn, development of such boundaries in various directions (see Fig. 3c and d). They are continuously formed by strain accumulation and microstructural heterogeneities, which evolve in each pass, accompanied by their intersection in grain interiors. The latter results in grain fragmentation followed by formation of the new fine grain structure with HABs at large strains. Note also that, in this way, the original microstructure of the predeformed alloy that contains the arrays of the low-to-moderate angle dislocation sub-boundaries (see Fig. 3a) may be very effective for development of new grains. It can be seen in Fig. 9 that the new fine grains start to rapidly develop in the current alloy just after the first pass through the die. In contrast, a similar strain-induced grain formation in as-cast and/or well-annealed Al alloys is usually retarded up to $\varepsilon_c \geqslant 2$ [17]. As was discussed in the previous work [32], the sub-boundaries in the initial structure of the present alloy may have resulted from DBs developed by prior extrusion and exist stably during heating just before ECAP. They can be frequently intersected with the DBs produced at the earlier stages of ECAP. This results in the more rapid evolution of new equiaxed crystallites with a stable grain size and therefore accelerates the kinetics of grain refinement [32].

On the other hand, an increasing deformation temperature may be very important for the rise in misorientation of the deformation-induced dislocation sub-boundaries. It has been reported recently [23] that the strong inhibition of recovery and homogenization of slip during ECAP of a dispersoid-containing alloy at ambient temperature makes DBs more diffuse and represses their transformation into HABs. In contrast, a high deformation temperature may give a greater possibility for the lattice dislocations to rearrange within the boundaries of DBs to transform them into permanent boundaries, which then increase their misorientation with further straining [22,23]. Furthermore, randomization of texture in fine-grained regions during warm-to-hot ECAP of the present alloy (see Fig. 6) allows us to assume that transformation of low-angle boundaries into large-angle ones may occur through the grain rotation caused by the grain boundary sliding (GBS) that can also be attributed to the increasing deformation temperature [38]. Note that the Al–Mg–Sc alloy with the average size of about 1 μm exhibits moderate superplastic properties in a wide strain rate interval at 300 °C [20], which supports this assumption. GBS can start to occur in the newly evolved grain structure along all layered boundaries of DBs, which primarily acquire high-angle misorientations [38]. The progressive rotation of the crystallites surrounded

by high- and low-angled boundaries can promote an increase in the misorientation of low-angle boundaries and their rapid conversion into HABs[6] [26,38].

Finally, it is important to note in Figs. 9–11 that V_{rex} and Θ_{ave} in fine-grained regions are gradually increased during grain refinement, while d_{rex} remains essentially stable at moderate and high strains. Such dependencies may be considered to be specific features of strain-induced grain structures, which are typical of cDRX [26]. It can be concluded therefore that new fine grains evolved during warm-to-hot ECAP of the present Al alloy resulted from a series of strain-induced continuous reactions; this is essentially similar to cDRX.

4.2. Development of the coarse-grained structural component

We can conclude from the present observations that the development of the coarse-grained structure in the Al–Mg–Sc alloy during ECAP at 300 °C can result from static recrystallization, which occurs through annealing of the as-deformed material by its exposure in the ECAP channel and/or reheating between passes. It should be noted that, due to the features of the ECAP technique, the microstructure developed by warm and hot ECAP should always be affected by a superposition of deformation and annealing processes [13,21]. First, it is unfortunately not possible to quench the sample immediately after its transition through the deformation zone. Namely, the shear deformation occurs by ECAP only in the intersection plane of the channels, while the material remains under the static annealing conditions inside the heated die both before arrival at and after leaving the deformation zone. Second, a spontaneous static annealing may also occur between ECAP passes, since the deformation temperature should be maintained and/or periodically restored during the whole ECAP procedure; this is inherent to the cyclic deformation mode of ECAP (see Fig. 1). The data in Fig. 11 clearly show that both the above-mentioned factors may exercise a significant influence on the structure of the ECAPed material and, therefore, must always be taken into account in the development of high-temperature ECAP regimes. However, it is rather surprising that the formation of "coarse" statically recrystallized grains takes place even in the material containing a respectable amount of fine coherent Al_3Sc particles, which can serve as very effective pinning agents and thus prevent recrystallization (e.g. [11,24,32]).

One criterion for the restraining effect of small intermetallic particles to influence recrystallization was proposed in Refs. [26,46] in terms of the restrained force of the particles, F_r, and the driving force for recrystallization, F_d. When the particles are randomly distributed, i.e. not preferably associated with grain boundaries or sub-boundaries, these can be defined as:

$$F_r = 1.5f\gamma/R \quad (1)$$

and

$$F_d = 0.5Gb^2\Delta\rho \quad (2)$$

where f is the volume fraction of particles, γ is the grain boundary energy, R is the particle radius, G is the shear modulus, b is the Burgers vector and $\Delta\rho$ is the dislocation density.

4.2.1. Restrained force

To evaluate the restrained force of the Al_3Sc particles, F_r, the following values were used: the grain boundary energy, $\gamma = 0.3\ J\ m^{-2}$ [47]; the volume fraction of the Al_3Sc phase in Al at 300 °C and the 0.3 wt.% Sc, in accordance with the lever rule, $f = 7.06 \times 10^{-3}$ [48]; and the particle radius, $R \sim 5 \times 10^{-9}$–10^{-8} m (see Section 2). The calculation resulted in F_r values lying in the interval $\sim 3 \times 10^5$–$6 \times 10^5\ N\ m^{-2}$. Also F_r should be increased to $\sim 6 \times 10^5$–$10^6\ N\ m^{-2}$, because it is known that the coherent particles are twice as effective in pinning grain boundaries compared with incoherent ones of the same size [26]. In addition, it is worth noting that solute drag can also hinder grain growth in the present alloy [26,49,50]. This may be due to the reduced boundary motility resulting from segregations of Mg- and impure atoms associated with the grain boundary [49]. It is apparent, however, that at $T \sim 0.6T_m$ the effect of solute on grain boundary migration is relatively small compared with that of coherent dispersoids [26], and thus it is not included in the quantitative analysis here.

4.2.2. Driving force

For the present deformation conditions, the values of the parameters for the calculation of F_d are given as follows: Burgers vector, $b = 2.8 \times 10^{-10}$ m [51]; shear modulus at 300 °C, $G = 2.16 \times 10^{10}\ N\ m^{-2}$ [51]. Substitution of these values in Eq. (2) leads to $F_d \sim 10^5\ N\ m^{-2}$ for $\Delta\rho = 10^{14}\ m^{-2}$ and $F_d \sim 10^6\ N\ m^{-2}$ for $\Delta\rho = 10^{15}\ m^{-2}$.

For the occurrence of recrystallization, it was proposed that $F_d \geqslant F_r$ [26,46], i.e. $\Delta\rho$ must be at least $\geqslant 6 \times 10^{14}\ m^{-2}$. Thus, despite the very approximate nature of the calculations, a very high stored dislocation density is apparently required to "trigger" recrystallization in the present Al–Mg–Sc alloy. It is also worth noting that Al alloys with high stacking-fault energy are normally considered to be "recovery materials", in which dynamic and/or static recovery operating extensively under warm-to-hot deformation conditions can effectively decrease the dislocation density stored during deformation and suppress recrystallization [26].

However, certain areas with an enhanced dislocation density can develop in the present alloy (see Figs. 5 and 7); therefore, the static recrystallization takes place

under warm-to-hot ECAP conditions. This may be caused by very inhomogeneous shear deformation with intense DBs that are introduced by the ECAP, as shown, for instance, in Fig. 3, and the reduced mobility of the lattice dislocations due to their strong interaction with the Al_3Sc particles (see Fig. 8a) and also the Mg atoms present in the solid solution, as discussed above. Because of the low rate of recovery, ECAP carries a high density of dislocations. Also note that the development of the statically recrystallized grains is more likely to occur in the mantle regions, where the strain gradients are greater [21,34,52].

Additional driving force for the "coarse" grain development may also be associated with the energy of the pre-existed grain boundaries [26,36,50] stored in the mantle regions. It can be clearly seen in Figs. 2b and 3b that formation of new recrystallized grains after the first ECAP pass starts to occur in the place of a fine-grained structure, which either is inherited from the microstructure present in the original mantle regions (Figs. 2a and 3a) and/or develops there in the early stage of ECAP.[7] As the (sub)grain size in the mantle regions, d, is relatively small (i.e. ~1–4 μm), this driving force, which is approximately $3\gamma/d$ [26,50], may be locally as high as $2–9 \times 10^5$ N m^{-2}, i.e. roughly equal to F_r. The (sub)grains present in the mantle regions may, therefore, be of major importance in providing pre-existing nuclei for static recrystallization, which contribute to the very rapid recrystallization kinetics taking place during "keeping" time after straining.

On the other hand, the occurrence of recrystallization accompanied by the grain boundary migration may, in turn, weaken the restraining effect of the Al_3Sc phase. It has been pointed out [26] that the passage of a high-angled boundary through a coherent particle results in the particle losing coherency. This may lead in turn to the rapid particle coarsening due to coagulation, as it was noticed in Fig. 7b, and, hence, may decrease F_r. At larger strains, this creates a strong possibility for "coarse" recrystallized grains to regenerate easily in the same local places after each ECAP pass.

Thus, ECAP of a heavily alloyed Al alloy may produce the high local driving force for static recrystallization under warm-to-hot deformation conditions and that can start to occur in some places of the deformation microstructure during "keeping" time in the ECAP channel and/or reheating between ECAP passes, when increased deformation temperature provides a large potential for grain boundary migration [26]. In contrast, in other places, where the microstructural conditions are not satisfied with the inequality $F_d \geqslant F_r$, i.e. the stored dislocation density is lower and/or the restraining effect of secondary particles is larger, the deformation microstructure remains essentially stable and no static recrystallization takes place. Instead, the progressive evolution of the microstructure may occur through a gradual strain accumulation within DBs in each ECAP pass and result in a transformation of their boundaries into high-angle ones in accordance with cDRX, as discussed in Section 4.1.

5. Conclusions

Microstructural evolution in a commercial Al–6% Mg–0.3% Sc alloy subjected to ECAP by route A to a total strain of 12 at 300 °C was examined in this work. The main results can be summarized as follows:

(1) A bimodal grain structure with grain sizes of about 1 and 8 μm and volume fractions of 0.3 and 0.6, respectively, develops during ECAP at moderate-to-high strains. Development of the two structural components with significantly different grain sizes results from the simultaneous operation of cDRX, occurring during deformation, and static recrystallization, which occurs during each ECAP pass by exposure of the as-deformed material in the ECAP channel keeping at 300 °C and reheating between ECAP passes.

(2) Intense shear deformation applied during each ECAP pass results in high strain/misorientation gradients and introduces DBs in original grain interiors. Structural changes in some parts of the deformation microstructure are characterized by evolution of these DBs, followed by formation of new fine grains at high strains in accordance with continuous reactions that are similar to cDRX.

(3) Coarser statically recrystallized grains are formed in the original mantle regions, developed during previous thermomechanical treatment, and in some parts of the grain interiors to consume areas with high local dislocation density. In the current heavily alloyed Al–Mg–Sc alloy, an enhanced driving force for recrystallization is provided even under warm-to-hot deformation conditions due to strong localization of plastic deformation introduced by ECAP and inhibition of recovery by the presence of coherent dispersion particles and a high concentration of Mg atoms in the solid solution.

(4) An important feature of the ECAP technique at elevated temperatures is that the ECAPed samples always undergo a spontaneous static annealing during their transition through the ECAP-die. This annealing may affect the microstructural development under warm-to-hot ECAP conditions remarkably and, therefore, should be taken into account by the development of the high-temperature ECAP regimes.

References

[1] Valiev RZ, Islamgaliev RK, Alexandrov IV. Prog Mater Sci 2000;45:103.
[2] Segal VM. Mater Sci Eng A 1995;197:157.
[3] Iwahashi Y, Horita Z, Nemoto M, Langdon TG. Acta Mater 1997;45:4733.
[4] Humphreys FJ, Prangnell PB, Bowen JR, Gholinia A, Harris C. Phil Trans Roy Soc Lond A 1999;357:1663.
[5] Valiev RZ, Langdon TG. Prog Mater Sci 2006;51:881.
[6] Iwahashi Y, Horita Z, Nemoto M, Langdon TG. Metal Mater Trans A 1998;29:2503.
[7] Prangnell PB, Bowen JR, Gholinia A. In: Dinesen AR, Eldrup M, Juul Jensen D, Linderoth S, Pedersen TB, Pryds NH, et al., editors. Proceedings of the 22nd Riso international symposium. Roskilde, Denmark: Riso National Laboratory; 2001. p. 105.
[8] Pithan C, Hashimoto T, Kawazoe M, Nagahora J, Higashi K. Mater Sci Eng A 2000;280:62.
[9] Yamashita A, Yamaguchi D, Horita Z, Langdon TG. Mater Sci Eng A 2000;287:100.
[10] Kaibyshev R, Sitdikov O, Mazurina I, Lesuer D. In: Chandra T, Higashi K, Suryanarayama C, Tome C, editors. Proceedings of Thermec '2000 international conference. J Mater Proc Tech-CD Version (Special issue); 2001.
[11] Lee S, Utsunomiya A, Akamatsu H, Neishi K, Furukawa M, et al. Acta Mater 2002;50:553.
[12] Goloborodko A, Sitdikov O, Sakai T, Kaibyshev R, Miura H. Mater Trans 2003;44:766.
[13] Chen YC, Huang YY, Chang CP, Kao PW. Acta Mater 2003;51:2005.
[14] Cao WQ, Godfrey A, Liu Q. Mater Sci Eng A 2003;361:9.
[15] Vinogradov A, Washikita A, Kitagawa K, Kopylov VI. Mater Sci Eng A 2003;349:318.
[16] Wang YY, Sun PL, Kao PW, Chang CP. Scripta Mater 2004;50:613.
[17] Goloborodko A, Sitdikov O, Kaibyshev R, Miura H, Sakai T. Mater Sci Eng A 2004;381:121.
[18] Furuno K, Akamatsu H, Oh-ishi K, Furukawa M, Horita Z, Langdon TG. Acta Mater 2004;52:2497.
[19] Prangnell PB, Bowen JR, Apps PJ. Mater Sci Eng A 2004;375–377:178.
[20] Musin F, Kaibyshev R, Motohashi Y, Itoh G. Metal Mater Trans A 2004;35:2383.
[21] Popovic M, Verlinden B. Mater Sci Technol 2005;21:606.
[22] Kaibyshev R, Shipilova K, Musin F, Motohashi Y. Mater Sci Eng A 2005;396:341.
[23] Apps PJ, Berta M, Prangnell PB. Acta Mater 2005;53:499.
[24] Ferry M, Hamilton NE, Humphreys FJ. Acta Mater 2005;53:1079.
[25] Liu Q, Juul Jensen D, Hansen N. Acta Mater 1998;46:5819.
[26] Humphreys FJ, Hatherly M. Recrystallization and related annealing phenomena. Oxford: Elsevier; 2004.
[27] Belyakov A, Sakai T, Miura H, Tsuzaki K. Philos Mag A 2001;81:2629.
[28] Filatov YA, Yelagin VI, Zacharov VV. Mater Sci Eng A 2000;280:97.
[29] Davydov VG, Rostova TD, Zakharov VV, Filatov YA, Yelagin VI. Mater Sci Eng A 2000;280:30.
[30] Appel F, Wagner R. Mater Sci Eng R 1998;22:187.
[31] Xing J, Soda H, Yang X, Miura H, Sakai T. Mater Trans 2005;46:1646.
[32] Sitdikov O, Sakai T, Avtokratova E, Kaibyshev R, Kimura Y, Tsuzaki K. Mater Sci Eng A 2007;444:18.
[33] Channel 5: User Manual, written by Day A and Trimby P with assistance from Mehnert K and Neumann B. HKL Technology; 2001.
[34] Sitdikov O, Sakai T, Goloborodko A, Miura H, Kaibyshev R. Philos Mag 2005;85:1159.
[35] Kocks UF, Tome CN, Wenk HR. Texture and anisotropy. Cambridge: Cambridge University Press; 1998.
[36] Molodova X, Gottstein G, Winning M, Hellmig RJ. Mater Sci Eng A 2007;460–461:204.
[37] Suwas S, Toth LS, Fundenberger J-J, Eberhardt A, Skrotzki W. Scripta Mater 2003;49:1203.
[38] Yang X, Miura H, Sakai T. Mater Trans 2002;43:2400.
[39] Williams DB, Carter CB, editors. Transmission electron microscopy. New York: Plenum Press; 1996. p. 289.
[40] Mackenzie JK. Biometrika 1958;45:229.
[41] Wang J, Iwahashi Y, Horita Z, Furukawa M, Nemoto M, et al. Acta Met 1996;44:2973.
[42] Morris DG, Munoz-Morris MA. Acta Mater 2002;50:4047.
[43] Mulders B, Zehetbauer M, Gottstein G, Les P, Shafler E. Mater Sci Eng A 2002;324:244.
[44] Langdon TG. Mater Sci Eng A 2007;462:3.
[45] Ringeval S, Piot D, Desrayaud C, Driver JH. Acta Mater 2006;54:3095.
[46] Manohar PA, Ferry M, Chandra T. ISIJ Int 1998;38:913.
[47] Murr F. Interfacial phenomena in metals and alloys. Reading (MA): Addison-Wesley; 1975.
[48] Marquis EA, Seidman DD. Acta Mater 2001;49:1909.
[49] Liu F, Kirchheim R. Thin Sol Films 2004;466:108.
[50] Driver JH. Scripta Mater 2004;51:819.
[51] Frost HJ, Ashby MF. Deformation-mechanism maps: the plasticity and creep of metals and ceramics. Oxford: Pergamon Press; 1982.
[52] Belyakov A, Gao W, Miura H, Sakai T. Metal Mater Trans A 1998;29:2957.